BIBECHANA
Vol. 23, No. 1, January 2026, 1-7

ISSN 2091-0762 (Print), 2382-5340 (Online)
Journal homepage: http://nepjol.info/index.php/BIBECHANA
Publisher:Dept. of Phys., Mahendra Morang A. M. Campus (Tribhuvan University)Biratnagar

Structural, magnetic phase stability, and electronic properties of Co_2RuSb Heusler compound

Prakash Khatri[1,2], **N. P. Adhikari**[1,*]

[1]*Central Department of Physics, Tribhuvan University, Kirtipur 44613, Kathmandu, Nepal*
[2]*Department of Physics, Siddhanath Science Campus, Tribhuvan University, Mahendranagar 10406, Nepal*
[*]Corresponding author. Email: narayan.adhikari@cdp.tu.edu.np

Abstract

The properties of Co_2RuSb were studied using DFT with the PBE-GGA functional for exchange-correlation energy. The most stable structures are identified by examining four distinct atomic configurations: $L2_1$-I, $L2_1$-II, XA-I, XA-II. Phase stability analysis in these configurations reveals that the ferromagnetic (FM) phase is more favorable than the antiferromagnetic (AFM) and nonmagnetic (NM) phases. Among all the considered structural and magnetic configurations, the compound prefers the XA-I type structure with a ferromagnetic (FM) ground state. The phonon dispersion curve, showing no imaginary frequencies, indicates that the Co_2RuSb compound is dynamically stable. From Born's stability criteria for elastic constants, Co_2RuSb is mechanically stable, exhibiting ductile behavior, and possess high melting temperatures. The spin-polarized band structures calculated with GGA reveal metallic behavior for both spin channels. The inclusion of on-site Coulomb interaction (U) via GGA + U might be interesting to explore in Co_2RuSb to examine its potential for spintronic applications.

Keywords: Heusler phases, Spintronics, Density functional theory, Magnetic properties. .

Article information
Manuscript received: August 15, 2025; Revised: September 18, 2025; Accepted: September 19, 2025
DOI https://doi.org/10.3126/bibechana.v23i1.83181

1 Introduction

Modern technologies in the field of spintronics and thermoelectrics are revolutionizing the world and getting a lot of attention of researchers. Spintronic devices hold promising applications in areas such as information technology, data storage, magnetic sensors, spin transistors, and memory devices [1–3]. Heusler alloys exhibiting half-metallicity are attractive for spintronic applications due to their 100% spin polarization, high Curie temperature, and ferromagnetic nature, whereas those with semiconducting and non-magnetic characteristics are well-suited for thermoelectric applications [4–6]. Among the different types of Heusler alloys, full Heusler compounds (X_2YZ) are ternary intermetallics made up of two transition metals (X and Y) and one main group element (Z), typically crystallizing in the $L2_1$ structure with the $Fm\bar{3}m$ space group [7]. In these compounds, all four atomic positions: (0, 0, 0), $(\frac{1}{2}, \frac{1}{2}, \frac{1}{2})$, $(\frac{1}{4}, \frac{1}{4}, \frac{1}{4})$, and $(\frac{3}{4}, \frac{3}{4}, \frac{3}{4})$ are fully occupied by atoms [7–9]. Half-metallic (HM) materials exhibit different spin orientations in the two spin channels, showing semiconducting or insulating behavior in one spin direction and metallic behavior in the other, and thus hold great potential for spin

generation, as the up and down-spin electrons can be treated as two separate currents [6,9].

In the quest for magnetic Heusler phases, we have reviewed the reported literature on various Co-based compounds, including Co_2YZ (Z = S, Ge, Se) [6], CO_2ZrZ (Z=Al, Si, Ga and Sn) [10], and Co_2FeZ (Z = Al, Ga, Si, Ge, S, Se and Te) [11]. The theoretical studies on these Co-based full Heusler alloys predict half-metallic behavior with high spin polarization and large magnetic moments, which are essential for spintronic applications [6, 10, 11]. Most of these compounds have a valence electron count different from 24 exhibit a total magnetic moment (μ) following the Slater–Pauling rule, given by $\mu = (N_V\text{-}24)$, where N_V is the number of valence electrons per formula unit [12]. These studies motivate us for the exploration of novel and previously unexplored Co-based compounds. After a thorough investigation, we found that the properties of the full Heusler compound Co_2RuSb have not yet been explored in the literature, either experimentally or theoretically. Therefore, we aimed to explore structural, magnetic phases and electronic properties of compound Co_2RuSb.

The structure of the paper is as follows: Section 2 describes the computational details, Section 3 presents the main results and discussion, and the final section provides the conclusions and concluding remarks of the present study.

2 Computational Details

The structural, electronic, and magnetic properties of the compound were systematically examined using density functional theory (DFT) as implemented in Quantum ESPRESSO (version 7.2) [13], employing a plane-wave basis set. The exchange-correlation interactions were taken into consideraion using the Perdew–Burke–Ernzerhof (PBE) generalized gradient approximation (GGA) [14]. The optimized crystal structure was visualized using XcrySDen [15]. A kinetic energy cutoff of 70 Ry and a charge density cutoff of 700 Ry were used, with a $10 \times 10 \times 10$ Monkhorst–Pack [16] k-point mesh chosen based on convergence tests for kinetic energy and k-points. The diagonalization method "david" was employed with a mixing factor of 0.3, along with Marzari–Vanderbilt smearing [17] of width 0.005 Ry throughout the calculations. Furthermore, spin-polarized calculations were carried out for different magnetic configurations, including ferromagnetic and antiferromagnetic states. k-points were sampled along the high-symmetry path $\Gamma \rightarrow X \rightarrow W \rightarrow K \rightarrow L \rightarrow U \rightarrow W \rightarrow L \rightarrow K$ within the first Brillouin zone (BZ) of the reciprocal lattice for band structure. The total and partial density of states (DOS and PDOS) were evaluated with a denser k-point mesh of $30 \times 30 \times 30$. Phonon dispersion calculations based on density functional perturbation theory (DFPT) [18] with a $2 \times 2 \times 2$ q-point mesh were conducted to evaluate the dynamical stability of the compound. The mechanical stability and related properties were evaluated using the thermo_pw code implemented in the Quantum ESPRESSO suite [19].

3 Results and Discussion

3.1 Structural stability

Full Heusler compounds have the chemical sructure X_2YZ, where X and Y are transition metals and Z is a main group element. The atoms occupy four interpenetrating face-centered cubic (fcc) sublattices at the Wyckoff positions A (0, 0, 0), B ($\frac{1}{4}$, $\frac{1}{4}$, $\frac{1}{4}$), C ($\frac{1}{2}$, $\frac{1}{2}$, $\frac{1}{2}$), and D ($\frac{3}{4}$, $\frac{3}{4}$, $\frac{3}{4}$). Table 1 presents the atomic arrangements for four structural types: $L2_1$-I, $L2_1$-II, XA-I, and XA-II. In the $L2_1$-I structure, Co atoms occupy the B and D sites, while Ru and Sb are positioned at C and A, respectively. In contrast, the $L2_1$-II structure has the same Co atom positions, but the C and A sites are swapped, i.e., occupied by Sb and Ru. In the inverse XA-I structure, the inequivalent Co1 and Co1 atoms occupy the A and B sites, while Ru and Sb are located at the C and D sites, respectively. In the XA-II structure, Co1 and Co1 are positioned at the A and C sites, with Ru and Sb occupying the B and D sites, respectively. The optimized atomic structures of the conventional unit cell of the compounds corresponding to the four structural types—$L2_1$-I, $L2_1$-II, XA-I, and XA-II are depicted in Figure 1(a-d).

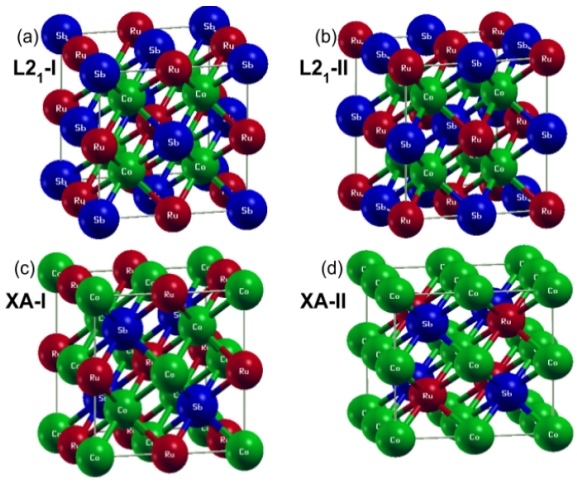

Figure 1: Conventional cubic unit cells of Co_2RuSb in various structural configurations (a) $L2_1$-I, (b) $L2_1$-II, (c) XA-I, and (d) XA-II), visualized using XcrySDen.

Table 1: Wyckoff positions for different structure types.

Structure type	Wyckoff positions			
	A	**B**	**C**	**D**
$L2_1$-I	Sb	Co	Ru	Co
$L2_1$-II	Ru	Co	Sb	Co
XA-I	Co1	Co2	Ru	Sb
XA-II	Co1	Ru	Co2	Sb

To determine the most stable structural configuration, the ground-state energy was minimized using the Murnaghan equation of state [20] ,

$$E(V)=\mathrm{E}_0+\frac{\mathrm{BV}}{B'}\left[\frac{1}{B'-1}\left(\frac{V_0}{V}\right)^{B'}+1\right] \quad (1)$$

for all four structural types ($L2_1$-I, $L2_1$-II, XA-I, and XA-II), which are presented in Figure 2(a-d).

The optimized lattice parameters obtained from energy minimization, followed by variable-cell relaxation, along with the corresponding total energies for different magnetic configurations. Their values for non-magnetic (NM), ferromagnetic (FM), and antiferromagnetic (AFM) for the four structural types ($L2_1$-I, $L2_1$-II, XA-I, and XA-II), are summarized in Table 2. The total energies obtained for the $L2_1$-I and $L2_1$-II structural types across their respective magnetic configurations are nearly identical and also comparable to that of the XA-II type. However, the total energies corresponding to the XA-I structural type are the lowest among all the configurations considered. Therefore, based on our observations, the XA-I structure is identified as the most stable configuration, with the ferromagnetic phase being the energetically preferred magnetic state like in Co_2FeS and Co_2FeTe [11]. Consequently, further calculations of dynamical stability, electronic structure, and magnetic properties were carried out based on the optimized lattice parameter (11.4973 Bohr (6.0841 Å)) of the ferromagnetic phase in the XA-I structural configuration.

3.2 Dynamical stability

The dynamical stability of compound was checked using phonon dispersion along the high-symmetry path $\Gamma \rightarrow X \rightarrow W \rightarrow K \rightarrow L \rightarrow U \rightarrow W \rightarrow L \rightarrow K$ in the BZ, as presented in Figure 3. The absence of imaginary frequencies along all high-symmetry directions of BZ confirms dynamical stability of both investigated compounds. Co_2RuSb has four atoms in its primitive unit cell, which leads to 12 phonon branches: three are low-frequency acoustical, and remaining nine are high-frequency optical modes. The acoustic and optical phonon branches are closely spaced, with an overlap between the highest acoustic and lowest optical frequencies. This indicates a high phonon scattering probability, which may lead to low thermal conduction by phonon in the compounds.

Table 2: Summary of the calculated lattice parameter a_0 (Å) and total energy E (Ry). The '*' symbol denotes the most stable structure.

Structure type	**Magnetic state**	**Lattice parameter a (Å)**	**Energy (Ry)**
$L2_1$-I	NM	11.3924	-365.71815389
$L2_1$-I	FM	11.5021	-365.74820362
$L2_1$-I	AFM	11.4531	-365.73749311
$L2_1$-II	NM	11.3917	-365.71815269
$L2_1$-II	FM	11.5021	-365.74820361
$L2_1$-II	AFM	11.4527	-365.73749312
XA-I	NM	11.4132	-365.74745959
XA-I*	FM	11.4973	-365.78427124
XA-I	AFM	11.4980	-365.75461190
XA-II	NM	11.3909	-365.71815227
XA-II	FM	11.5018	-365.74820363
XA-II	AFM	11.4533	-365.73749370

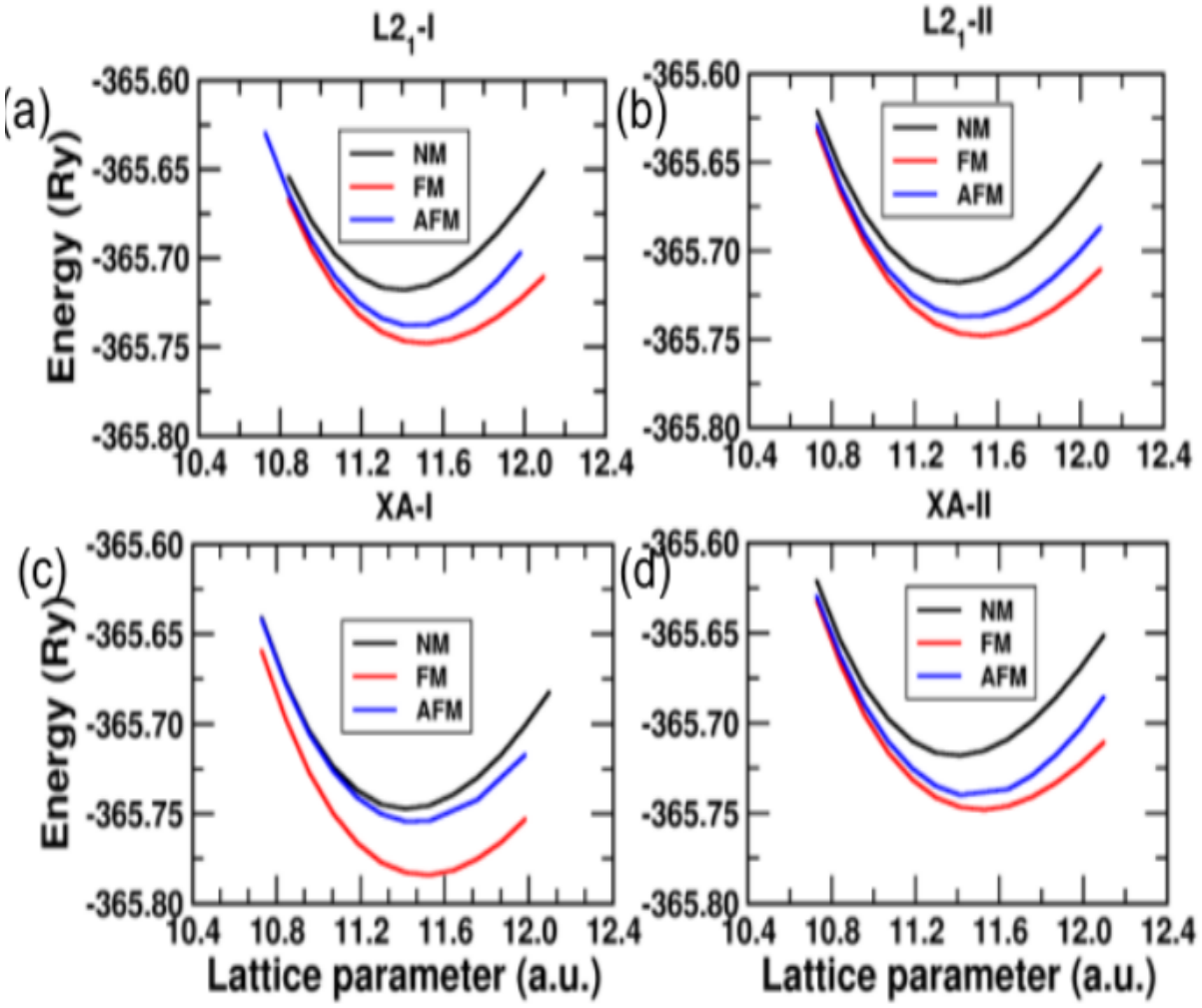

Figure 2: Energy (Ry) VS lattice parameter (a.u.) for all four structural types (a) L2$_1$-I, (b) L2$_1$-II, (c) XA-I, and (d) XA-II.

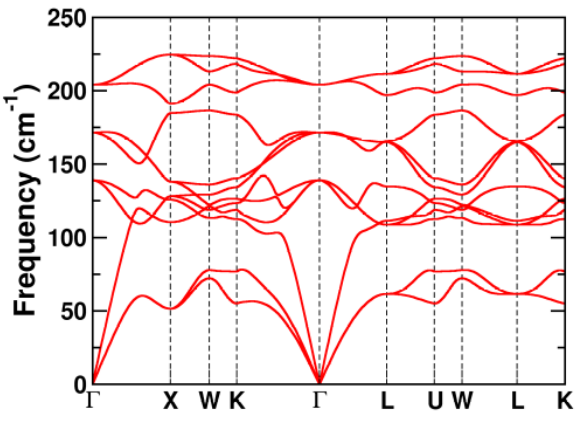

Figure 3: Phonon dispersion plot of the compound CoRuSb.

3.3 Mechanical stability

For practical applications, a material must exhibit mechanical stability and superior mechanical properties, which we have assessed for Co_2RuSb through the evaluation of its elastic constants. For a crystal with cubic symmetry, 3 independent elastic constants C_{11}, C_{12}, and C_{44} are sufficient to assess its mechanical stability. According to Born's criteria for mechanical stability of cubic crystals [21], the following conditions must be satisfied: $C_{11}>0$, $C_{44}>0$, C_{11} - C_{12} > 0, and $C_{11}+2C_{12}>0$. The calculated C_{ii}'s of compound are C_{11}=189.53 GPa, C_{12}=178.61 GPa, and C_{44}=81.26 GPa. From Born's stability criteria, the compound is mechanically stable.

Furthermore, we assessed the ductility or brittleness of the compound using Pugh's ratio (B/G) and Poisson's ratio (ν), where the criteria for ductility are positive Cauchy pressure (C=C_{12}-C_{44}), B/G>1.75, and ν>0.26 [22, 23]. Since the compound exhibits B/G=3.57, ν=0.37, and a positive C, we conclude that the compound is ductile.

The bulk modulus (B), shear modulus (G) and Young's modulus (Y) were calculated using Voigt-

Reuss-Hill approximation [24],

$$\mathrm{B}=\frac{C_{11}+2C_{12}}{3} \tag{2}$$

$$\mathrm{G}=\frac{G_v+\mathrm{G}_R}{3} \tag{3}$$

with

$$G_v=\frac{C_{11}+\mathrm{C}_{12}+\mathrm{C}_{44}}{3}$$

and

$$G_R=\frac{5\left(C_{11}-C_{12}\right)C_{44}}{4C_{44}+3\left(C_{11}-C_{12}\right)}$$

$$\mathrm{Y}=\frac{9\mathrm{BG}}{3\mathrm{B}+\mathrm{G}} \tag{4}$$

The calculated bulk modulus (B=182.25 GPa), Young's modulus (Y=88.07 GPa), and shear modulus (G=31.66 GPa) indicate that the compound possesses good mechanical rigidity, stiffness, and toughness, making it suitable for practical applications [24]. Using the empirical relation $\mathrm{T_m}$ = [553K + (5.91K/GP a)$\mathrm{C_{11}}$] ± 300K for cubic crystals [25], the predicted melting temperature of 1673.12 K indicates that the compound is potentially suitable for high-temperature thermoelectric applications.

3.4 Electronic structure and magnetic properties

In this section, we present and discuss the band structure of Co_2RuSb HHs for both spin-up and spin-down channels, calculated along path $\Gamma \rightarrow X \rightarrow W \rightarrow K \rightarrow L \rightarrow U \rightarrow W \rightarrow L \rightarrow K$ in the BZ using the PBE-GGA approach. The corresponding band structures for the spin up and down channels are shown in the figure 4. The spin up band structure exhibits metallic characteristics, as the multiple bands intersect the Fermi level without a band gap. Similarly, in the spin down channel, the band structure also shows metallic behavior, with bands overlapping the Fermi level, as observed in the spin-up channel. The presence of band crossings at the Fermi level in both spin channels destroys the half-metallic character of Co_2RuSb under PBE-GGA. A similar behavior has been reported for Co_2YGe when analyzed using the same exchange-correlation functional [6].

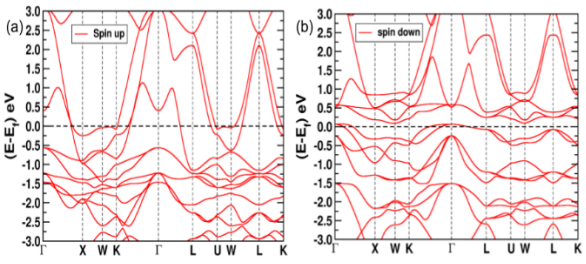

Figure 4: Electronic band structures of the Co_2RuSb compound for (a) spin up (b) spin down channels, calculated along high-symmetry directions of BZ.

Furthermore, we analyzed the electronic DOS and PDOS of Co_2RuSb for both spin up and down channels. We observe that the minority spin channel significantly contributes to the total DOS at Fermi level E_F, whereas the majority spin channel shows an almost negligible contribution, with only a few states near E_F. To understand the atomic contributions to the total DOS, we also computed the PDOS, as in Figure 5. The PDOS reveals that 4d states of Ru contribute significantly near E_F in spin up channel. The spin down channel is predominantly contributed by the Co1 and Co_2 3d states, along with the 4d states of the Ru atom. However, the 5p states of Sb contribute negligibly in both spin channels.

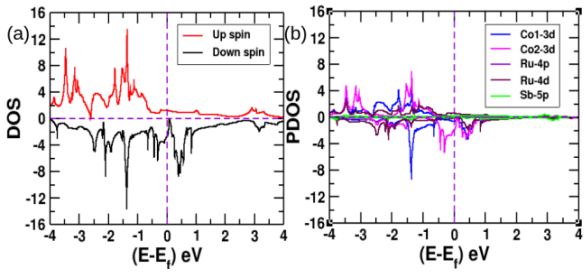

Figure 5: (a) Total DOS (b) projected DOS for Co_2RuSb in both spin channels.

For the stable FM-XA-I phase, the magnetic moment is 3.32 μ_B/cell, which deviates than that expected from the Slater–Pauling rule (SPR). However, this deviation is still relevant, as SPR applies mainly to cubic, stoichiometric Heusler alloys in the half-metallic limit [26]. For example, Shakil et al. [6] reported that Co_2YGe shows metallic behavior with a magnetic moment of 3.24 μ_B in GGA, deviating from the SPR, but it drops to 0.98 μ_B with GGA+U, consistent with SPR. With Hubbard U, the magnetic moment may follow the SPR like in the compound Co_2YGe [6], but this needs further investigation. In addition, spin polarization measures how strongly the spins are oriented along a

given direction and are given as [10, 27]:

$$SP = \frac{DOS\ (EF\uparrow) - DOS\ (EF\downarrow)}{DOS\ (EF\uparrow) - DOS\ (EF\downarrow)} \quad (5)$$

For our compound, DOS↑(EF) = 1.23 and DOS↓(EF) = 2.25, giving a spin polarization of 29.31%. However, GGA+U could induce half-metallicity and 100% spin polarization, as seen in Co_2RuGe [6], which has lower SP without Hubbard U but reaches 100% SP with its inclusion.

Although the PBE-GGA functional indicates metallic behavior of the compound due to the overlap of electronic states, which disrupts half-metallic character of compound, the inclusion of the Hubbard U correction might significantly influence its electronic and magnetic properties. GGA+U can improve the description of Co_2RuSb by better accounting for electron correlations in the localized d-orbitals of Co and Ru. It might open a gap in one spin channel, increasing spin polarization and potentially making the material half-metallic with more accurate magnetic moments closer to experimental or Slater–Pauling values. Therefore, investigating the band structure of Co_2RuSb using the GGA + U approach, by incorporating a Coulomb potential, would be of great interest for future studies.

4 Conclusion

The structural and magnetic phase stability, as well as the electronic properties of Co_2RuSb, were carried out using density functional theory. The energy versus lattice parameter optimization was performed for all possible stable magnetic phases for optimized lattice parameter. Based on the analysis of various structural types and magnetic phase stabilities, Co_2RuSb is found to be most stable in the XA-I type structure with a ferromagnetic ground state. Phonon dispersion and elastic constant analysis confirm that compound is dynamically and mechanically stable. The compound is mechanically ductile and has a high melting point, indicating its suitability for high temperature applications. The presence of multiple band crossings at the Fermi level for both spin channels, without any band gap, reveals the metallic nature of the compound and destroys the half-metallicity under the PBE-GGA approximation. From the PDOS, Ru-4d states dominate near E_F in the spin-up channel, while Co_1/Co_2-3d and Ru-4d states prevail in spin-down channel; Sb-5p states show negligible contribution in both. Applying GGA + U may induce half-metallicity in Co_2RuSb, making it a valuable subject for future study.

Acknowledgments

PK acknowledges the support provided by UGC Nepal through the PhD grant (award no. PhD-79/80-S&T-14) and the partial assistance received under NT-14 from ICTP/EAU.

References

[1] X. P. Wei, Y. L. Zhang, X. W. Sun, T. Song, P. Guo, Y. Gao, and J. B. Deng. Exchange interactions and curie temperatures in fe2 niz compounds. *Journal of Alloys and Compounds*, 694:1254–1259, 2017. doi:10.1016/j.jallcom.2016.10.105.

[2] F. Casper, T. Graf, S. Chadov, B. Balke, and C. Felser. Half-heusler compounds: novel materials for energy and spintronic applications. *Semiconductor Science and Technology*, 27(6):063001, 2012. doi:10.1088/0268-1242/27/6/063001.

[3] K. Elphick, W. Frost, M. Samiepour, T. Kubota, K. Takanashi, H. Sukegawa, and A. Hirohata. Heusler alloys for spintronic devices: review on recent development and future perspectives. *Science and Technology of Advanced Materials*, 22(1):235–271, 2021. doi:10.1080/14686996.2020.1812364.

[4] H. Zenasni, H. I. Faraoun, and C. Esling. First-principle prediction of half-metallic ferrimagnetism in mn-based full-heusler alloys with highly ordered structure. *Journal of Magnetism and Magnetic Materials*, 333:162–168, 2013. doi:10.1016/j.jmmm.2013.01.003.

[5] J. Kübler, A. R. William, and C. B. Sommers. Formation and coupling of magnetic moments in heusler alloys. *Physical Review B*, 28(4):1745, 1983. doi:10.1103/PhysRevB.28.1745.

[6] M. Shakil, S. Mushtaq, I. Zeba, S. S. A. Gillani, M. I. Khan, H. Arshad, and M. Rafique. Structural, electronic, magnetic and thermoelectric properties of full heusler alloys co2yz (z= s, ge, se): A first principles calculation. *Physica B: Condensed Matter*, 602:412558, 2021. doi:10.1016/j.physb.2020.412558.

[7] S. Ahmed, M. Zafar, M. Rizwan, M. I. Khan, H. Arshad, J. Hai-Bo, and M. Shakil. Theoretical investigation of structural and magnetic properties of mntix (x= si, ge, se, te) half-heusler alloys. *Indian Journal of Physics*, 95(5):841–849, 2021. doi:10.1007/s12648-020-01739-x.

[8] S. Amari, S. Méçabih, B. Abbar, and B. Bouhafs. First-principles calculations of magnetic properties for cdcro2 under pressure. *Journal of Magnetism and Magnetic Materials*, 327:76–78, 2013. doi:10.1016/j.jmmm.2012.09.027.

[9] G. H. Fecher, H. C. Kandpal, S. Wurmehl, C. Felser, and G. Schönhense. Slater-pauling rule and curie temperature of co2-based heusler compounds. *Journal of Applied Physics*, 99(8), 2006. doi:10.1063/1.2167629.

[10] G. Remil, A. Zitouni, B. Bouadjemi, M. Houari, A. Abbad, W. Benstaali, and S. Bentata. A potential full heusler thermoelectric material co2zrz (z= al, si, ga and sn) in low temperature: An ab-initio investigation. *Solid State Communications*, 336:114422, 2021. doi:10.1016/j.ssc.2021.114422.

[11] M. Saleem and M. Shakil. A comprehensive investigation of structural and magnetic phase stability, electronic, magnetic and thermoelectric properties of co2fez (z= al, ga, si, ge, s, se and te) full heusler alloys. *Solid State Communications*, 355:114947, 2022. doi:10.1016/j.ssc.2022.114947.

[12] Q. L. Fang, J. M. Zhang, and K. W. Xu. Magnetic properties and origin of the half-metallicity of ti2mnz (z= al, ga, in, si, ge, sn) heusler alloys with the hg2cuti-type structure. *Journal of Magnetism and Magnetic Materials*, 349:104–108, 2014. doi:10.1016/j.jmmm.2013.08.030.

[13] P. Giannozzi, O. Andreussi, T. Brumme, O. Bunau, M. B. Nardelli, M. Calandra, and S. Baroni. Advanced capabilities for materials modelling with quantum espresso. *Journal of Physics: Condensed Matter*, 29:465901, 2017. doi:10.1088/1361-648X/aa8f79.

[14] J. P. Perdew, K. Burke, and M. Ernzerhof. Generalized gradient approximation made simple. *Physical Review Letters*, 77:3865, 1996. doi:10.1103/PhysRevLett.77.3865.

[15] A. Kokalj. Xcrysden—a new program for displaying crystalline structures and electron densities. *Journal of Molecular Graphics and Modelling*, 17:176–179, 1999. doi:10.1016/S1093-3263(99)00028-5.

[16] H. J. Monkhorst and J. D. Pack. Special points for brillouin-zone integrations. *Physical Review B*, 13:5188, 1976. doi:10.1103/PhysRevB.13.5188.

[17] N. Marzari, D. Vanderbilt, A. De Vita, and M. C. Payne. Thermal contraction and disordering of the al (110) surface. *Physical Review Letters*, 82:3296, 1999. doi:10.1103/PhysRevLett.82.3296.

[18] S. Baroni, S. De Gironcoli, A. Dal Corso, and P. Giannozzi. Phonons and related crystal properties from density-functional perturbation theory. *Reviews of Modern Physics*, 73:515, 2001. doi:10.1103/RevModPhys.73.515.

[19] A. D. Corso. thermo_pw. https://dalcorso.github.io/thermo_pw, 2024. Accessed: 08/10/2024.

[20] F. D. Murnaghan. The compressibility of media under extreme pressures. *Proceedings of the National Academy of Sciences*, 30:244–247, 1944. doi:10.1073/pnas.30.9.244.

[21] M. Born and R. Fürth. The stability of crystal lattices. iii: An attempt to calculate the tensile strength of a cubic lattice by purely static considerations. *Mathematical Proceedings of the Cambridge Philosophical Society*, 36:454–465, 1940. doi:10.1017/S0305004100017503.

[22] I. N. Frantsevich. *Elastic constants and elastic moduli of metals and insulators. Reference book*. 1982.

[23] S. F. Pugh. Xcii. relations between the elastic moduli and the plastic properties of polycrystalline pure metals. *The London, Edinburgh, and Dublin Philosophical Magazine and Journal of Science*, 45(367):823–843, 1954. doi:10.1080/14786440808520496.

[24] Liang Zuo, Michel Humbert, and Claude Esling. Elastic properties of polycrystals in the voigt-reuss-hill approximation. *Applied Crystallography*, 25(6):751–755, 1992. doi:10.1107/S0021889892004874.

[25] M. E. Fine, L. D. Brown, and H. L. Marcus. Elastic constants versus melting temperature in metals. *Scripta Metallurgica*, 18:951–956, 1984. doi:10.1016/0036-9748(84)90267-9.

[26] S. Bhattacharjee and S. C. Lee. A general rule for predicting the magnetic moment of cobalt-based heusler compounds using compressed sensing and density functional theory. *Journal of Magnetism and Magnetic Materials*, 563:169818, 2022. doi:10.1016/j.jmmm.2022.169818.

[27] F. Dahmane, B. Doumi, Y. Mogulkoc, A. Tadjer, D. Prakash, K. D. Verma, and R. Khenata. Investigations of the structural, electronic, magnetic, and half-metallic behavior of co2mnz (z= al, ge, si, ga) full-heusler compounds. *Journal of Superconductivity and Novel Magnetism*, 29(3):809–817, 2016. doi:10.1007/s10948-015-3357-2.